Ambient Electromagnetic Energy Harvesting Circuit using Rectennas Manufactured with Stereolithography Resin

Xuan Viet Linh Nguyen, Tony Gerges, Jacques Verdier, Philippe Lombard, Michel Cabrera, Bruno Allard
Univ Lyon, INSA Lyon, Université Lyon1, Ecole Centrale de Lyon, CNRS, Ampère, UMR5505,
69621 Villeurbanne, France
xuan.nguyen@insa-lyon.fr

Jean-Marc Duchamp, Philippe Benech
Univ. Grenoble-Alpes, CNRS, Grenoble INP, G2Elab, 21 avenue des martyrs, CS 90624, 38031 Grenoble, France

Acknowledgements

Authors would like to appreciate Murata Integrated Components for their helps for our project (IPCEI INCA Nano 2022).

Keywords

«Electromagnetic Energy Harvester», «Elastic/Plastic deformation», «Energy management system», «Additive Manufacturing»

Abstract

The paper discusses exploratory results to validate main performances of an ambient electromagnetic field energy harvester implemented on a limited surface of non-dedicated polymer object fabricated using 3D Molded Interconnect Devices (3D MID) technology or Plastronics. The prototype is experimented with discrete devices (-7.5 dBm minimum total input RF power, 14.75% global efficiency).

Introduction

Nowadays, Internet of Things (IoT) devices become more and more popular in our life with many practical applications (sensors, smartwatches, smartphones, etc.). Nevertheless, the massive development of these devices leads a dramatic issue of requiring a huge amount of batteries which always contain many harmful components to the environment and to human's health. Therefore, many researches about replacing the batteries by the cleaner energy, such as vibrations, light, pressure, temperature [1] have been studied. Since the number of wireless communication devices increases rapidly, the ambient electromagnetic power density improves consequently. Developing the self-powered devices by harvesting the Radio Frequency (RF) energy becomes an interesting solution for replacing the batteries [2]–[5]. As the shell of devices are used mostly to protect the components inside and rarely for electronic purposes, it is convenient to implement the electrical functions, the RF components, the antennas, etc. on the surface of the 3D plastic packages.
We report here a system to harvest ambient electromagnetic energy, implemented on the surface skin of a 3D plastic object with the purpose of feeding a vehicle sensor for instance. The system consists in a RF-to-DC rectifier used to convert electromagnetic (EM) waves to DC energy and a Power Management Circuit (PMC) used to boost and regulate the rectified voltage of rectifier. The plastic object is fabricated using 3D MID methods: Stereolithography – an additive manufacturing method and electroless metallization.

The system is studied firstly with discrete components for verification purpose prior to the design of an integrated PMC with a companion capacitive Interposer to aggregate the various capacitors required in the circuit operation. A magnetic device is considered in the PMC that is too complex to integrate yet. The number of components to assemble on the object skin to create the function should be small as brazing a component on the object surface is challenging.
This paper is organized as follows. The RF-to-DC rectifier is presented in the first section. The method of fabricating, metallizing and choosing the components for the circuit will be described shortly in this section as well. Afterwards, a study about the electrical relation between the rectifier and the PMC to optimize the total efficiency of the system will be mentioned. Then, the principle of the PMC as well as the measurement results of the system in discrete form will be studied in the third section. Finally, a conclusion and perspectives will be given.

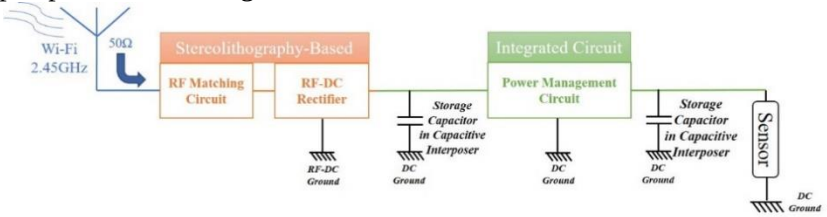

Fig. 1: Schematic of the targeted system

Stereolithography-based RF-to-DC rectifier

Fabrication of 3D printed and metallized rectifier

The polymer substrates are 3D-printed with a Stereolithography (SLA) printer Form 3 from Formlabs (Fig. 2). The high temperature resin FLHTAM02 from Formlabs is selected thanks to its good thermal resistance (around 238°C) for future brazing operation. After printing, the parts are cleaned in isopropanol to remove resin residuals and then UV cured with thermal post-processing to enhance their mechanical strength.
The electronic circuit and the antennas are fabricated by metallizing the substrates by copper Electroless Deposition (ELD) (method detailed in [6]). The thickness of the deposited copper is measured with X-ray fluorescence (Bowman (Serial B-XRF). The average measured value is (7 ± 1) µm. The electroless copper conductivity is measured with four-point-probes used with S-302 stand (Signatone) and attached to a Keithley (2450 SourceMeter). The measurements are carried out over 10 samples. The measured conductivity is around $(45 \pm 4.5) \times 10^6$ S/m.

RF-to-DC rectifier design

RF-to-DC rectifier plays a crucial role of converting the electromagnetic waves into DC power in the concept of a radio frequency energy harvester (RFEH) circuit. The proposed rectifier is a combination in parallel of four series topology rectifiers connected serially to RF chokes, which are used to prevent the load from RF signals, with one common storage capacitor (C_{common}) at the output of the circuit. The schematic and the realized circuit are illustrated in Fig. 2. The rectifying diode is the low-barrier Schottky diode SMS7630-079LF from Skyworks Solutions Inc. selected due to its low threshold voltage. In each branch of rectifier, to match the circuit to 50 Ω and to ensure the closed loop of DC current in the branch, a shorted circuit stub is employed. The load is chosen as 1 kΩ where the rectifier achieves its Maximum Power Point Tracking (MPPT) condition. C_{common} is set as 1 µF to optimize the operation of the PMC [7]. The storage capacitors in the circuit are the Surface Mounted Device (SMD) components of Murata used in Power Applications. Discrete SMD components are selected in the first step. Once the circuit is validated, they can be replaced by a capacitive interposer fabricated by Murata Integrated Passives to reduce the size as well as to improve the performances of the circuit. The circuit is simulated and optimized with the aid of Advanced Design System (ADS) Momentum for an input power of -20 dBm at the frequency of 2.45 GHz at each branch.

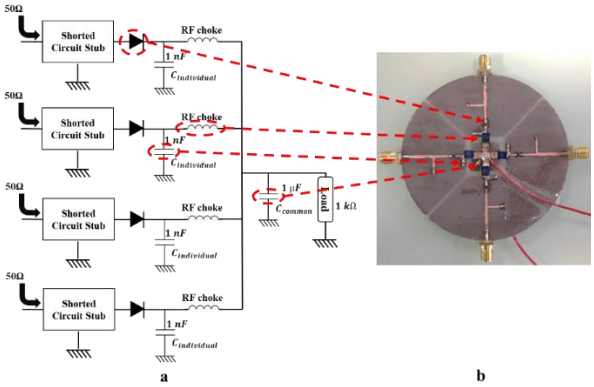

Fig. 2: Stereolithography-based RF-to-DC rectifier (a. Schematic of designed rectifier; b. Realized circuit)

Measuring the internal impedance of rectifier

Method of identifying the internal impedance

The MPPT condition of the rectifier is obtained when its output load is identical to the internal impedance of the circuit. This internal impedance is defined as the junction resistance, also known as Zero Bias Resistance (ZBR), of the rectifying diode at high frequencies [8]. Identifying the value of this resistance is necessary in order to optimize the efficiency of the system.

The relation between the incident power (P_i) at the input of the rectifier, the reflected loss (P_r) from the impedance matching condition and the transmitted power (P_t) towards the rectifying diode is given as

$$P_i = P_r + P_t \ (1)$$

Additionally, the RF-to-DC conversion efficiency of the circuit (η_{RF-DC}) can be expressed as

$$\eta_{RF-DC} = \frac{V_{out}^2}{R_L P_i} \ (2)$$

where, V_{out} is the rectified voltage at the load (V), R_L is the load (Ω) and P_i is the incident power at the input of the rectifier (W).

It is worthy to notice that, when a well-designed matching circuit is applied at a pre-defined input power and frequency, P_r can be neglected. Then, the following approximation is led

$$P_i = P_t \ (3)$$

The Eq. (2) is then written as

$$\eta_{RF-DC} = \frac{V_{out}^2}{R_L P_t} \ (4)$$

The internal impedance of the rectifier can be pointed out from η_{RF-DC} in variation of the load. However, when the load varies, P_r will not stay constant since the matching circuit is served for only one value of load, frequency and input power. P_t is not identical consequently. This leads the impacts to the accuracy of measured results. Ideally, for each value of load, frequency and input power, a corresponding matching circuit should be used. Literally, this approach requires a very complicated manipulation. Here, a method of determining the internal impedance of the rectifier using only one rectifier circuit for any measurement is considered. The method is based on changing P_i and measuring P_r so that P_t determined from Eq. (1) reaches the desired value of input power where the

circuit is well-matched to 50 Ω and getting η_{RF-DC} for each value of load. For our measurements, we set P_t at different values, i.e. -30 dBm, -20 dBm, -10 dBm and 0 dBm for the frequency of 2.45 GHz. The measurement schematic and experimental setup are illustrated in Fig. 3.

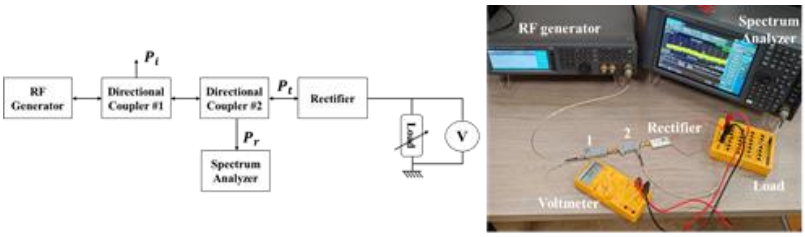

Fig. 3: The proposed method of identifying the internal impedance of the rectifier (a. Measurement schematic; b. Experimental setup (1 – Directional Coupler #1 used to measure the incident power P_i, 2 – Directional Coupler #2 used to measure the reflected loss P_r)).

The measurements are carried out on a mono-diode series topology rectifier with the Schottky diode SMS7630-079LF shown in Fig. 4.

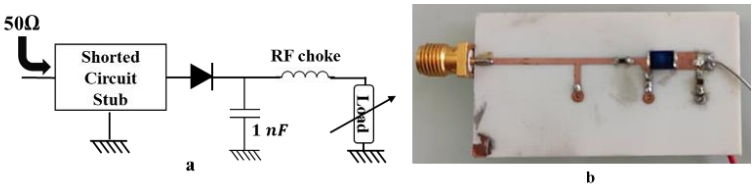

Fig. 4: The measured mono-diode series topology (a. Schematic of the circuit; b. Realized rectifier)

The simulated and measured results are plotted in Fig. 5. The internal impedance of the mono-series diode rectifier varies as functions of the input power of the circuit. The values of this impedance and η_{RF-DC} are respectively 5 kΩ (3.5 %) at -30 dBm, 3 kΩ (15.7 %) at -20 dBm, 2.5 kΩ (34.4 %) at -10 dBm and 2 kΩ (45.1%) at 0 dBm. In fact, the measured rectified voltage is sensitive to the accuracy of the source power level. 0.1 dB of shifting of the source power impact up to 2% the measured rectified voltage.

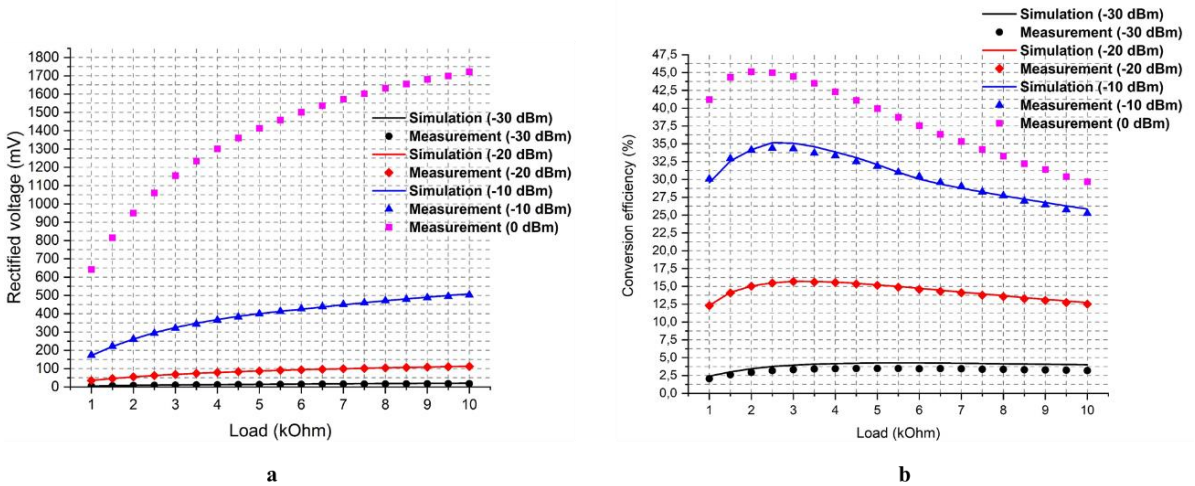

Fig. 5: The measured results of mono-diode series rectifier used to identify the internal impedance (a. Measured rectified voltage; b. Corresponding conversion efficiency)

In [5], this value varies as function of the input power level, which are 2.6 kΩ at 0 dBm, 4 kΩ at -20 dBm and 7.2 kΩ at -35 dBm. However, the lossy impacts from the matching circuit are not concerned

in the measurements. In [8], authors show that the ZBR of this rectifying diode is around 5.1 kΩ at low current across the diode. In [9], a study of obtaining the optimal load of the rectifier at different temperature (from -20 °C to 30 °C) is carried out. At the ambient temperature (around 23 °C), ZBR of SMS7630 diode is from 6 kΩ to 7 kΩ at different input power level, which are from -40 dBm to -20 dBm. Comparing to our state-of-art, our measured results are very close to them. The difference between the results may come from the deployed method and/or the variation of the measured diode models.

Internal impedance of 4-port rectifier

The desired circuit is a RF-to-DC rectifier of four inputs illustrated in Fig. 2. The internal impedance of the circuit should be determined to maximize its conversion efficiency. The topology of each branch is mono-series diode, the Thevenin equivalent schematic of our 4-port rectifier in term of DC circuit is presented in Fig. 6. Since, the branches are linked in parallel, with the hypothesis is that if the input power at each input is lower than -30 dBm, it will be considered as zero, the equivalent internal impedance of the circuit ($Z_{circuit}$) can be calculated ideally as

$$\frac{1}{Z_{circuit}} = \sum_{i=1}^{4} 1/Z_{int\ imp_i} \quad (5)$$

where $Z_{int\ imp_i}$ is the internal impedance of branch "i" at a defined input power at 2.45 GHz (Ω).

In fact, in situation of energy harvesting, the input power of each branch is not nor constant nor identical (from -30 dBm to 0 dBm), $Z_{circuit}$ will not fixed at a certain value consequently. Here, our proposed circuit is preferred to have ability of working in all possibilities. The value of $Z_{circuit}$ of all possibilities are calculated and plotted in Fig. 6. According to Fig. 6, the values of $Z_{circuit}$ are gathered mostly around the value of 1 kΩ. This value is therefore chosen as the value of the load.

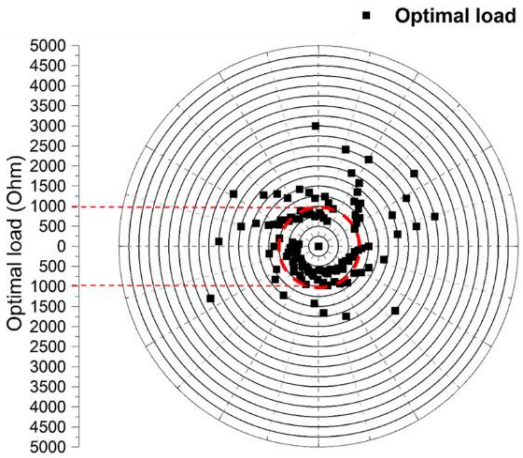

Fig. 6: The calculated optimal load of the 4-port rectifier

Discrete Power Management Circuit

The idea of our PMC was introduced in [10]. The circuit in Fig. 7 consists of a self-oscillating Armstrong converter for cold start-up and a Flyback converter in Discontinuous-Conduction Mode (DCM) for continuous operation. A low-consumption oscillator TS3002 of Silicon Labs is used to generate the switching frequency for the Flyback converter and two Under-Voltage-Lock-Out (UVLO) circuits discriminate the circuit operation. A Flyback converter in DCM mode operates the Maximum Power Point Tracking (MPPT) conditions and features a better efficiency than the Armstrong's one. It should be noticed that the Flyback converter supplies the oscillator and a natural

feedback effect is obtained to track MPPT conditions. UVLO#1 is used to keep the Flyback converter operation during the variation of load. UVLO#2 has the role of regulating the output voltage.

A 2D circuit is fabricated with discrete components available on the market.

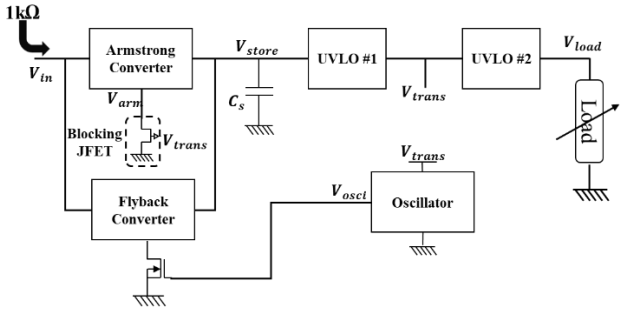

Fig. 7: Block diagram of the Power Management Circuit

The circuit has the following operation phases: Cold start, Transition from Amstrong to Flyback, Normal operation and Deactivation.

Cold start phase: When the voltage across the storage capacitor C_{s1} reaches to a minimum starting voltage [10], the Armstrong converter oscillates and boosts the voltage and stores the energy in another storage capacitor C_{s2}. The ideal minimum starting voltage (V_{start_min}) can be estimated as [10]

$$V_{start\_min} \approx (2I_{DSS}R_S + |V_p|)/m \quad (1)$$

Where, R_s is the impedance of source of circuit (Ω), I_{DSS} and V_p are Zero-Gate Voltage Drain Current (A) and Threshold Voltage (V) respectively of JFET used in Armstrong and m is the amplification ratio of transformer used in Armstrong. The selected JFET is J201 ($I_{DSS} = 0.6\ mA$ and $V_p = -0.6\ V$) and the transformer is WE750311681 from Würth Elektronik ($m = 10$). Thus, the estimated minimum voltage is 0.18 V.

Transition phase: the Armstrong converter keeps working until the voltage across C_{s2} reaches the closed threshold voltage ($V_{closed1}$) of UVLO#1 (1.2 V). Once UVLO#1 is closed, C_{s2} will feed the oscillator (V_{trans}) to start the Flyback converter. Simultaneously, V_{trans} will feed also the Gate of the blocking JFET (J177) to deactivate Armstrong converter.

Normal operation phase: the Flyback converter is self-supplied as long as the voltage V_{trans} is high enough to keep the oscillator working. The voltage across C_{s2} continues to increase until it reaches the closed threshold voltage ($V_{closed2}$) of UVLO#2 (1.57 V). When UVLO#2 is closed, C_{s2} feeds the load. When the load supply voltage (V_{load}) decreases below the opened threshold voltage ($V_{opened2}$) of UVLO#2 (1.4 V), UVLO#2 disconnects the load, and C_{s2} will start to re-charge.

In this phase of operation, the input impedance of the circuit (R_{input}) is determined as [7]

$$R_{input} = 2L_1 f_{sw}/D^2 \quad (2)$$

Where, L_1 is the primary inductance of the transformer (H), f_{sw} and D are respectively the switching frequency (Hz) and the duty cycle (50%) generated by the oscillator. A LPD6235-205 transformer from Coilcraft is selected due to its high primary inductance (2 mH). As presented previously, in order to achieve the optimal efficiency, the input impedance of the circuit should be fixed at 1 kΩ, the MPPT load of the rectifier. Therefore, f_{sw} and D of the oscillator are set as 65 kHz and 50%.

Deactivation phase: When V_{store} is lower than the opened threshold voltage ($V_{opened1}$) of UVLO#1 because of the degradation of the RF input voltage for example, UVLO#1 will disconnect the Flyback convertor. The Armstrong converter will be reactivated as long as the input voltage of circuit is higher than 0.26 V.

Measurement results

The PMC is tested with the rectifier in Fig. 2 and the total input power of -7.5 dBm of the rectifier at the frequency of 2.45 GHz. The measured input voltage of PMC is 0.264 V, where the circuit starts to operate. The electrical behavior of the PMC is presented in Fig. 8.

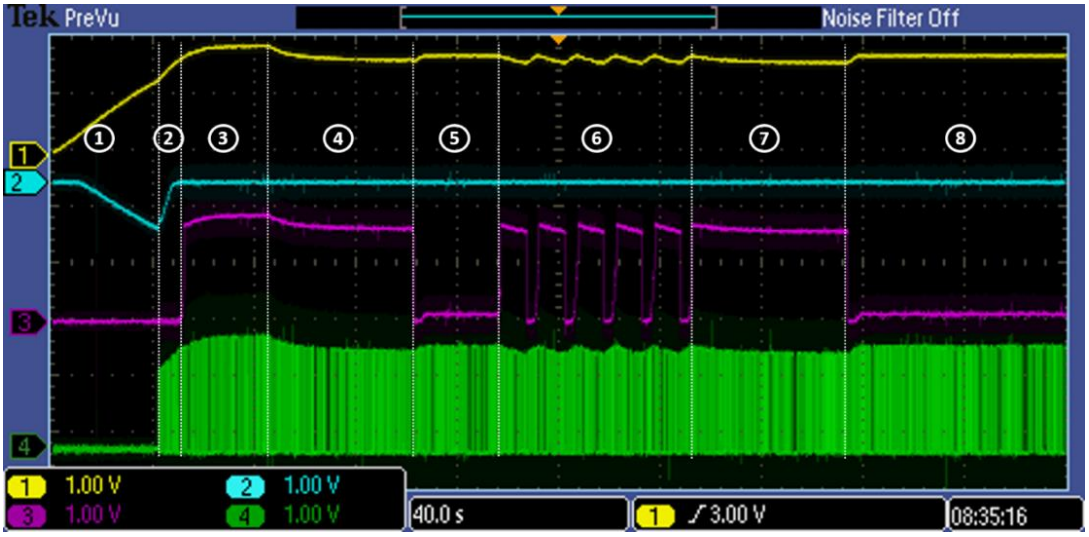

Fig. 8: The measured results of discrete Power Management Circuit (Yellow: V_{store} ; Blue: V_{arm} ; Purple: V_{load} ; Green: V_{osci})

In Fig. 8, the yellow curve presents the variation of voltage of storage capacitor C_{s2} ; the blue curve shows if the Armstrong circuit activated or deactivated; the purple curve is the voltage of the load; the green curve is the signal generated by the oscillator of the Flyback converter.

1) First, the load at the PMC's output is 1 MΩ. The circuit is currently in "cold start" phase. The storage voltage V_{store} across the storage capacitor C_s is pulled up due to the Armstrong converter. During the process, this voltage is not high enough to close UVLO#1 ($V_{closed1}$ < 1.2 V), thus, the Flyback converter is not activated yet and V_{load} stays at zero.

2) When V_{store} reaches $V_{closed1}$, the Flyback converter is activated and the Armstrong converter is turned off. However, V_{store} is still lower than the threshold voltage $V_{closed2}$ (1.57 V) of UVLO#2. Therefore, there is no supply of the load. The circuit is in "transition" phase.

3) The Flyback converter increases V_{store}. When V_{store} is higher than $V_{closed2}$, the load is supplied (V_{load} is identical to V_{store}). It should be noticed that the load is 1 MΩ. The transmission of energy from C_s to the load occurs immediately. The circuit is in "normal operation" phase.

4) The load is reduced to 100 kΩ. V_{load} is reduced to 1.62 V, but still higher than the threshold voltage $V_{opened2}$ (1.4 V) of UVLO#2. The PMC input power is sufficiently high to cover the circuit losses and the load consumption.

5) The load is then set to 10 kΩ. V_{load} drops until it is lower than $V_{opened2}$. UVLO#2 is then opened, the Flyback converter increases until V_{store} is higher than $V_{closed2}$. UVLO#2 is closed again. Since, the load is low, its consumption and the losses in the circuit increase [7], [10], this explains the slight output voltage. The Flyback converter keeps in operation as UVLO#1 is closed.

6) The load is fixed at 80 kΩ, i.e. the limit value of load in "normal operation" phase. We have a discontinuous supply of the load. This load consumes more energy, thus, C_s discharges rapidly.

7) The load is set to 100 kΩ with a similar operation as in case 4.

8) The load is set to 10 kΩ with a similar operation as in case 5.

The output voltage is 1.62 V for a load of 100 kΩ with an input voltage of 0.264 V in "*normal operation"* phase. The PMC boost ratio is then 6.14. The global efficiency of the system (η_{global}) in "*normal operation"* phase and for 100 kΩ at 0.264V input voltage is 14.75%.

The amplified voltage is around 1.62 V for a load of 100 kΩ with an input of 0.264 V. Hence, the amplified ratio of PMC is 6.14. The global efficiency of system (η_{global}) can be calculated as

$$\eta_{global} = V_{load}^2/(R_{load} \times P_{RF\ total}) = 1.62^2/(100k\ \times 10^{-3.75}) = 14.75\%$$

Conclusion

The discrete component circuit validates the operation of the rectifier and the PMC. The global efficiency is 14.75 % for a total power level of -7.5 dBm of the rectifier.

The performances' improvement of the circuit at the MPPT load depends on the capability of the rectifier with respect to the input power level as shown in Fig. 5 for one PMC. The other key element is the antenna gain. In addition, the efficiency of the Flyback used in the PMC is tributary on the electrical properties and the dimensions of the coupled inductance of the transformer [7].

The price of the energy harvesting circuit is a secondary issue compared to life-cycle assessment (LCA) of the device. Assembling of Armstrong and Flyback components is a good candidate for the energy harvesting applications [10] even though it requires a large number of components that contribute to a high level of gray energy. With the ambient EM energy available in the air [4], [11], during the life duration of the payload circuit, the harvested energy might be at least equal to its equivalent gray energy.

References

[1] S. Sudevalayam and P. Kulkarni, "Energy Harvesting Sensor Nodes: Survey and Implications," *IEEE Commun. Surv. Tutor.*, vol. 13, no. 3, pp. 443–461, 2011, doi: 10.1109/SURV.2011.060710.00094.

[2] E. Vandelle, D. H. N. Bui, T.-P. Vuong, G. Ardila, K. Wu, and S. Hemour, "Harvesting Ambient RF Energy Efficiently With Optimal Angular Coverage," *IEEE Trans. Antennas Propag.*, vol. 67, no. 3, pp. 1862–1873, Mar. 2019, doi: 10.1109/TAP.2018.2888957.

[3] "Design and experiments of a dual-band rectenna for ambient RF energy harvesting in urban environments - Khemar - 2018 - IET Microwaves, Antennas & Propagation - Wiley Online Library." https://ietresearch.onlinelibrary.wiley.com/doi/10.1049/iet-map.2016.1040 (accessed May 28, 2022).

[4] U. Muncuk, K. Alemdar, J. D. Sarode, and K. R. Chowdhury, "Multiband Ambient RF Energy Harvesting Circuit Design for Enabling Batteryless Sensors and IoT," *IEEE Internet Things J.*, vol. 5, no. 4, pp. 2700–2714, Aug. 2018, doi: 10.1109/JIOT.2018.2813162.

[5] S.-E. Adami *et al.*, "A Flexible 2.45-GHz Power Harvesting Wristband With Net System Output From −24.3 dBm of RF Power," *IEEE Trans. Microw. Theory Tech.*, vol. 66, no. 1, pp. 380–395, Jan. 2018, doi: 10.1109/TMTT.2017.2700299.

[6] T. Gerges *et al.*, "Investigation of 3D printed polymer-based heat dissipator for GaN transistors," in *2021 23rd European Conference on Power Electronics and Applications (EPE'21 ECCE Europe)*, Sep. 2021, p. P.1-P.9.

[7] A. Capitaine, "Récupération d'énergie à partir de piles à combustible microbiennes benthiques," Theses, Université de Lyon, 2017. Accessed: May 28, 2022. [Online]. Available: https://tel.archives-ouvertes.fr/tel-02090785

[8] S. Hemour *et al.*, "Towards Low-Power High-Efficiency RF and Microwave Energy Harvesting," *IEEE Trans. Microw. Theory Tech.*, vol. 62, no. 4, pp. 965–976, Apr. 2014, doi: 10.1109/TMTT.2014.2305134.

[9] X. Gu, L. Guo, S. Hemour, and K. Wu, "Optimum Temperatures for Enhanced Power Conversion Efficiency (PCE) of Zero-Bias Diode-Based Rectifiers," *IEEE Trans. Microw. Theory Tech.*, vol. 68, no. 9, pp. 4040–4053, Sep. 2020, doi: 10.1109/TMTT.2020.2992024.

[10] S.-E. Adami, “Optimisation de la récupération d’énergie dans les applications de rectenna,” phdthesis, Ecole Centrale de Lyon, 2013. Accessed: May 28, 2022. [Online]. Available: https://tel.archives-ouvertes.fr/tel-00967525
[11] H. Takhedmit, “Ambient RF power harvesting: Application to remote supply of a batteryless temperature sensor,” in *2016 IEEE International Smart Cities Conference (ISC2)*, Sep. 2016, pp. 1–4. doi: 10.1109/ISC2.2016.7580800.